Journal of Modern Techniques in Biology and Allied Sciences
This Content Available at www.lapinjournals.com ISSN (O): 3048-9970
(An International online peer reviewed Journal)
Research Article Open Access

SYNTHESIS AND CHARACTERIZATION OF A SELENIUM/CHITOSAN NANOCOMPOSITE AND ITS EFFECT ON HORIZONTAL TRANSFER OF ANTIBIOTIC-RESISTANCE GENES AMONG CLINICAL GRAM-NEGATIVE ISOLATES

OSAMAH RAJI MAL ALLAH*

Al-Qadisiyah director education, Ministry of education, Iraq

***CORRESPONDING AUTHOR**
Osamah Raji Mal Allah

Article History: Received: 28 July, 2026, Revised: 14 August, Accepted: 21 September, 2026

ABSTRACT
Antibiotic resistance is now spreading faster than new drugs can reach the clinic, and much of that spread is carried by plasmids that move between Gram-negative bacteria through conjugation. We prepared a selenium/chitosan nanocomposite (Se/CS NCs) by reducing sodium selenite with ascorbic acid in a dilute chitosan solution, and asked whether one material could both kill multidrug-resistant (MDR) clinical isolates and interrupt the horizontal transfer of resistance genes. The reaction turned brick-red within 18 min and gave an 87.4% yield. UV-Vis absorption peaked at 268 nm. XRD matched hexagonal selenium with a mean crystallite size of 32 nm, and FTIR showed a new Se-O/Se-N band near 615 cm^{-1} together with a weaker amine signal, which points to selenium anchored on the chitosan amino groups. The particles were semi-spherical and 48.6 ± 7.2 nm by TEM, with a zeta potential of +31.8 mV. Sixty isolates were collected, 78.3% of them MDR. Across a representative panel drawn from that collection the composite lowered the mean MIC to 29.7 µg/mL, well below selenium nanoparticles or chitosan on their own, and it was bactericidal (MBC/MIC = 2). At sub-inhibitory doses it cut the conjugation frequency from 4.7×10^{-3} to as low as 1×10^{-9}. The transfer genes *traA*, *traD*, *traI* and *traJ* were down-regulated while *finP* rose, and resistance genes such as $bla_{CTX\text{-}M\text{-}15}$, $bla_{NDM\text{-}1}$ and $bla_{OXA\text{-}48}$ were seldom recovered from transconjugants. The composite spared normal HFF-1 fibroblasts and the non-cancerous HEK-293 line (IC_{50} 312 µg/mL; selectivity index 9.75 against the 32 µg/mL MIC of most MDR isolates). Se/CS NCs thus work on two fronts, killing resistant cells and blocking the machinery that spreads resistance.

Keywords: *Selenium nanoparticles; Chitosan; Nanocomposite; Horizontal gene transfer; Plasmid conjugation; Multidrug resistance; Gram-negative bacteria.*

This article is licensed under a Creative Commons Attribution-Non-commercial 4.0 International License. Copyright © 2026 Author(s) retains the copyright of this article.

INTRODUCTION

The rise of antibiotic resistance has become one of the hardest problems in modern medicine. A recent global estimate linked bacterial resistance to almost five million deaths in a single year [1]. Gram-negative species carry much of this burden. *Escherichia coli*, *Klebsiella pneumoniae*, *Pseudomonas aeruginosa* and *Acinetobacter baumannii* are now routinely isolated with resistance to several drug classes at once, and options for treating them keep shrinking [2,3]. And the problem is made worse by opposition that won't stay put. Bacteria exchange resistance genes with their neighbours. The major pathway is conjugation, the direct transfer of plasmids from a donor to a recipient cell [4]. One transfer event can transform a sensitive strain into an MDR one, as a single conjugative plasmid can carry genes for extended-spectrum β-lactamases, carbapenemases and other characteristics [5]. Therefore, it is not enough to kill bacteria. It is equally important to reduce the circulation of resistance genes. Nanomaterials have attracted interest here because they target bacteria in ways that are difficult to resist

[6,7]. Selenium nanoparticles are of special importance. They are active against many diseases and selenium is an essential trace element, thus damage to host cells is often mild [8,9]. Chitosan contributes a second valuable property. It is a cationic biopolymer that can bind to bacterial surfaces and also stabilises tiny particles preventing them from clumping [10,11]. The combination of both should result in a material that is both more potent and easier to handle than each component alone [12,13].

Yet few studies have asked whether a selenium/chitosan composite can do more than kill cells, that is, whether it can also block the spread of resistance genes. This study set out to fill that gap. We prepared Se/CS NCs, characterised them in detail, tested them against clinical Gram-negative isolates, and measured their effect on conjugal transfer and on the genes that drive it.

2. MATERIALS AND METHODS

2.1. Chemicals and reagents

Sodium selenite (Na_2SeO_3), low-molecular-weight chitosan ([degree of deacetylation %], [molecular weight]), L-ascorbic acid, glacial acetic acid and sodium hydroxide were used as received from [supplier]. Mueller-Hinton broth and agar, and the reagents for molecular work, were of analytical grade [supplier]. All solutions were prepared in deionised water.

2.2. Preparation of the Se/CS nanocomposite

Chitosan was dissolved at 0.5% (w/v) in 1% (v/v) acetic acid and stirred until clear. Sodium selenite was added to a final concentration of 10 mM, giving a selenium-to-chitosan ratio of 1:3 (w/w). Ascorbic acid was then introduced as the reducing agent. The mixture was stirred at 400 rpm and held at 45 °C, and the pH was adjusted to 5.2 with 0.1 M NaOH. A brick-red colour appeared after about 18 min, which is the visual sign that Se(IV) has been reduced to elemental Se(0) [14,15]. Stirring continued for 45 min. The colloid was recovered by centrifugation at [xxxx] rpm for [xx] min, washed [n] times with deionised water and ethanol, and dried at [temperature]. The yield was calculated against the theoretical selenium mass.

2.3. Physicochemical characterisation

Formation of the composite was first followed by UV-Vis spectroscopy over 200-500 nm ([UV-Vis model]). Functional groups were examined by FTIR over 400-4000 cm^{-1} ([FTIR model]). The crystalline phase was determined by X-ray diffraction using Cu Kα radiation ([XRD model]) and the average crystallite size was calculated from the Scherrer equation. The morphology was studied using field emission scanning electron microscopy (FESEM) and transmission electron microscopy (TEM) ([microscope models]). The particle sizes were estimated from the micrographs. Hydrodynamic size and polydispersity were obtained by dynamic light scattering, and colloidal stability from the zeta potential ([analyser model]). Elemental composition was checked by energy-dispersive X-ray spectroscopy (EDX) [16].

2.4. Bacterial isolates and identification

Sixty non-duplicate Gram-negative isolates were collected from Diwaniya Teaching Hospital and the Maternity and Children Teaching Hospital, Al-Diwaniyah city, Iraq between January 2025 and December 2025. They came from urine, blood, wound, sputum, burn, ear and endotracheal samples. Species were identified by standard biochemical tests and confirmed with the VITEK 2 system (bioMérieux, Marcy-l'Étoile, France). Susceptibility to a panel of antibiotics was read by the Kirby-Bauer method and interpreted with CLSI breakpoints (CLSI M100, 35th ed., 2025). Isolates non-susceptible to at least one agent in three or more antimicrobial classes were classified as multidrug-resistant (MDR), and isolates non-susceptible to at least one agent in all but two or fewer classes as extensively drug-resistant (XDR), following the standard definitions [17]. The study was approved by the Research Ethics Committee of Diwaniya Teaching Hospital, Al-Diwaniyah, Iraq (approval no. DTH-2024-127).

2.5. Antibacterial activity (MIC and MBC)

Minimum inhibitory concentrations were determined by broth microdilution in 96-well plates. Se/CS NCs, plain selenium nanoparticles and chitosan were each tested over [range] µg/mL against a set of reference and MDR isolates. Plates were incubated at 37 °C for [16-20] h. The MIC was the lowest concentration with no visible growth. For the minimum bactericidal concentration, aliquots from clear wells were subcultured on agar, and the MBC was the lowest concentration that killed at least 99.9% of the inoculum. The MBC/MIC ratio was used to judge whether the effect was bactericidal or bacteriostatic. Reference strains (*E. coli* ATCC 25922, *K. pneumoniae* ATCC 700603 and *P. aeruginosa* ATCC 27853) were tested alongside the clinical isolates for quality control. Each test was run in [n] replicates.

2.6. Conjugation (mating) assay

The effect on horizontal transfer was measured in a broth mating assay [18,19]. An MDR clinical donor ([donor isolate code and species]) carrying a conjugative resistance plasmid of [replicon/incompatibility group] was mated with a plasmid-free recipient ([recipient strain, e.g., *E. coli* J53, sodium-azide resistant]). Donor and recipient were mixed at a [1:1] ratio and exposed to sub-inhibitory doses of Se/CS NCs (1/4 and 1/2 MIC), with selenium nanoparticles and chitosan at 1/4 MIC for comparison, and an untreated control. After [x] h at 37 °C, transconjugants were selected on plates containing the recipient marker plus an antibiotic keyed to the plasmid. The conjugation frequency was expressed as transconjugants per recipient (T/R).

2.7. Expression of transfer and quorum-sensing genes

To see how the composite acts, gene expression was measured by quantitative real-time PCR (RT-qPCR). Cells were exposed to a sub-inhibitory dose (1/2 MIC), and total RNA was extracted and reverse-transcribed [kit]. The transfer genes *traA*, *traD*, *traI* and *traJ*, the negative regulator *finP* and the outer-membrane gene *ompA* were measured in the enterobacterial donor ([donor isolate code]), since these are F-type plasmid and enterobacterial genes. The quorum-sensing genes *lasI* and *rhlR* were measured separately in a *P. aeruginosa* isolate ([isolate code]), because they occur only in that species. All primers are listed in Supplementary Table S1. Relative expression was calculated by the $2^{-\Delta\Delta Ct}$ method against [reference gene, e.g., 16S rRNA] and compared with the untreated control.

2.8. Detection of resistance genes in transconjugants

Transconjugants from the treated and untreated matings were screened by PCR for a set of clinically important resistance genes: $bla_{CTX\text{-}M\text{-}15}$, $bla_{TEM\text{-}1}$, $bla_{SHV\text{-}12}$, $bla_{NDM\text{-}1}$, $bla_{OXA\text{-}48}$, *qnrS*, *aac(6')-Ib-cr*, *sul1* and *tetA*. The frequency of each gene before and after treatment was recorded, and the drop was taken as a measure of blocked transfer. Primers and conditions are given in Supplementary Table S2.

2.9. Cytotoxicity (MTT assay)

Biocompatibility was assessed by the MTT assay on HFF-1 normal human foreskin fibroblasts and on HEK-293, a non-cancerous immortalised embryonic kidney line. Cells were treated for [24/48] h with Se/CS NCs over 16-1024 µg/mL. Viability was read at 570 nm and expressed as a percentage of the untreated control. The IC_{50} was interpolated from the dose-response curve, and a selectivity index (SI) was calculated as IC_{50} divided by the MIC recorded for most of the MDR clinical isolates.

2.10. Statistical analysis

Experiments were performed in [n] independent replicates and results are given as mean ± SD. Differences were tested by [one-way ANOVA with Tukey's post-hoc test / Student's t-test] in [software, version]. A p-value below 0.05 was taken as significant.

3. RESULTS AND DISCUSSION

3.1. Formation of the composite and optical properties

The synthesis was straightforward to see. The addition of ascorbic acid to the clear chitosan solution resulted in a brick-red colour at 18 min and the colour became darker as the reaction proceeded. This red hue is characteristic of elemental selenium colloids and represents the conversion of Se(IV) to Se(0) [14]. The reaction produced a good yield of 87.4%, which is excellent for an aqueous method at ambient pressure and indicates that chitosan was effective in trapping and retaining the developing particles. In practice, chitosan seems to have a double purpose. Its amino and hydroxyl groups bind selenite ions and provide a location for the reduction to begin. The same groups then surround the young particles and prevent them from getting too large. Ascorbic acid was chosen as the reductant, as it is mild, cheap and food grade, keeping the entire route green and avoiding the harsher agents employed in many chemical syntheses. The whole list of synthesis conditions is described in Table 1. UV-Vis spectroscopy supported this reading . A single well-defined absorption band was seen at 268 nm (Figure 2, inset), within the range reported for tiny selenium nanoparticles [8]. Selenium is a semiconductor, hence this band is due to interband and excitonic absorption, not to a typical surface plasmon. The band was rather narrow, with a width at half-height of 42 nm, which normally means a reasonably limited size range. No second peak at longer wavelength was seen therefore there was minimal evidence of big aggregates in the fresh colloid.

Table 01: Optimised conditions for the synthesis of the Se/CS nanocomposite and the resulting yield.

Parameter	Value	Unit / note
Se:CS ratio	1:3	w/w
Chitosan concentration	0.5	% w/v in 1% acetic acid
Na_2SeO_3 concentration	10	mM
Reducing agent	Ascorbic acid	Se(IV) -> Se(0)
Temperature	45	°C, 400 rpm
pH	5.2	adjusted with 0.1 M NaOH
Reaction time	45	min
Time to brick-red colour	18	min
Synthesis yield	87.4	% (mean ± 2.1)

3.2. Functional groups (FTIR)

The position of selenium on the polymer was investigated by FTIR (Figure 1, Table 2). Pristine chitosan presented the characteristic bands such as large O-H/N-H stretch at about 3450 cm−1, C-H stretch at about 2920 cm−1, amide I and amide II at around 1650 and 1560 cm−1, C-O-C stretch at about 1070 cm−1 and glycosidic ring band at 894 cm−1. The composite still had these traits, they were just moved. The broad O-H/N-H band shifted to 3420 cm−1 and the amide II band at 1548 cm−1 was decreased about a third of its strength. The coordination of the amino groups of chitosan to selenium is expected to result in both modifications [12,13]. The most clear new evidence was a band at 615 cm-1 which we relate to

Se-O/Se-N vibrations. This is lacking in plain chitosan and demonstrates the formation of a true chemical interaction, and not a simple physical mixing.

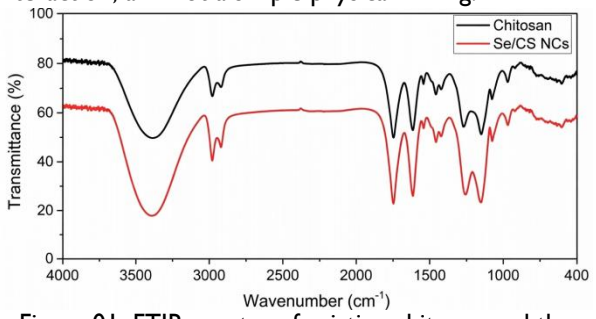

Figure 01: FTIR spectra of pristine chitosan and the Se/CS nanocomposite.

Table 02: FTIR band positions of chitosan and the Se/CS nanocomposite with assignments.

Band (cm^{-1})	Assignment	Change on composite formation
3420	O-H / N-H stretch	Shift from 3450; coordination with Se
2920	Aliphatic C-H stretch	Methylene groups
1642	C=O stretch (amide I)	Residual acetyl group
1548	N-H bending (amide II)	Intensity down ~30%; amine-Se interaction
1378	C-H bending	CH2, CH3
1078	C-O-C stretch	Glucosamine ring
896	β-1,4 glycosidic vibration	Characteristic of chitosan
615	Se-O / Se-N stretch	New band; confirms the composite

3.3. Crystalline phase and crystallite size (XRD)

The XRD pattern (Figure 2) simultaneously conveyed two meanings. A large hump at 2θ=23.5° corresponds to a semi-crystalline and partially amorphous fraction, perhaps the chitosan matrix and some poorly organised selenium. On top of this, a sequence of sharp reflections were observed at 29.7, 41.4, 43.7, 45.5, 51.8, 56.2 and 61.6°. These index neatly to the (101), (110), (102), (111), (201), (112) and (202) planes of hexagonal (trigonal) selenium with the (101) plane producing the greatest signal (Table 3). The clarity of these peaks implies that a large fraction of the selenium had crystallised into the stable t-Se phase [15]. The average crystallite size was calculated from the primary reflections by using the Scherrer equation and was found to be 32 nm, somewhat less than the particle size from microscopy, as expected since each particle can contain more than one crystalline domain. It is interesting to see the presence of diffuse background and well defined crystalline peaks. The amorphous fraction is often the more reactive one whereas the crystalline t-Se core provides the particles with shelf stability. Thus a substance that carries both may be stable on storage, but nevertheless release active species when it encounters a bacterial cell.

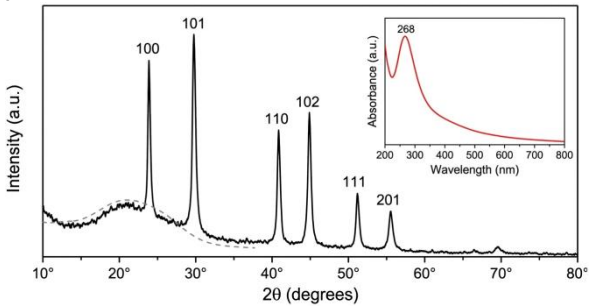

Figure 02: XRD pattern of the Se/CS nanocomposite; inset: UV-Vis. absorption spectrum.

Table 03: X-ray diffraction reflections of the Se/CS nanocomposite and Scherrer crystallite size.

2θ (°)	Relative intensity	Plane (hkl) / note
23.5	78	Broad; semi-crystalline Se
29.7	100	(101), hexagonal Se
41.4	46	(110)
43.7	38	(102)
45.5	32	(111)
51.8	24	(201)
56.2	20	(112)
61.6	18	(202)
Mean crystallite size	32 nm	Scherrer equation

3.4. Morphology, size, charge and composition

Electron microscopy showed semi-spherical, rather homogeneous particles (Figure 3). The rounded form and absence of sharp edges are typical of selenium produced in the presence of a capping polymer which restricts directional growth. Size study showed the mean TEM diameter was 48.6 ± 7.2 nm with the data ranged throughout 25-75 nm (Figure 4). Dynamic light scattering indicated a higher hydrodynamic size of 78 nm with a polydispersity index of 0.24. This difference between the two values is predicted, since DLS also measures the hydrated chitosan shell and any loose surface layer, while TEM measures the dense core . A PDI of 0.24 is still considered a fairly narrow, monodisperse preparation.

The zeta potential measured +31.8 mV. Generally, a value > +30 mV is read as a good colloidal stability and the positive sign is significant for the biology that follows: it encourages contact with the negatively charged surfaces of Gram negative bacteria [10,20]. The composition of the substance was validated by EDX (Figure 5) with the predominant element being selenium (38.4 wt%) followed by carbon (34.1 wt%),

oxygen (21.7 wt%) and nitrogen (5.8 wt%). The carbon, oxygen and nitrogen are provided by chitosan, and the detection of these elements with a significant selenium signal is consistent with a real Se/CS composite, not bare selenium.

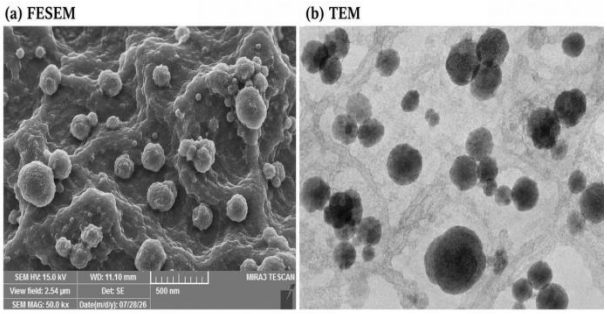

Figure 03. (a) FESEM and (b) TEM micrographs of the Se/CS nanocomposite. The two panels are placeholders; the authors will insert the recorded micrographs with their own scale bars. Mean diameter from TEM 48.6 ± 7.2 nm (n = [number of particles measured]).

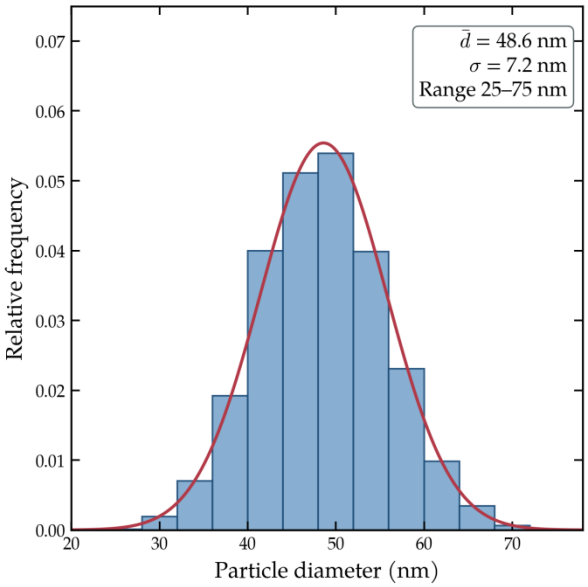

Figure 04: Particle-size distribution of the Se/CS nanocomposite from TEM measurements.

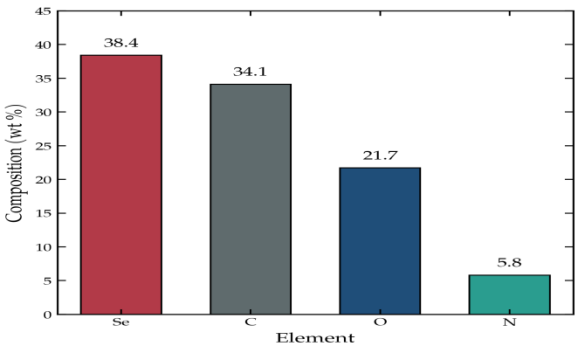

Figure 05: EDX elemental composition of the Se/CS nanocomposite.

3.5. Clinical isolates and their resistance profile

E. coli (22) and *K. pneumoniae* (18) constituted the majority of the 60 isolates, with P. aeruginosa (12) and A. baumannii (8) making up the remainder (Table 4). Most were resistant to many medication families. Altogether, 47 isolates (78.3%) were classified as MDR, with the highest proportion of MDR in A. baumannii (87.5%) and K. pneumoniae (83.3%). This pattern is consistent with observations in Iraqi and regional hospitals reporting the frequent occurrence of carbapenem- and β-lactamase-producing Gram-negatives [2,3,21]. Such a collection will severely test any new agent.

Table 04: Distribution of the 60 clinical Gram-negative isolates and their MDR rates.

Species	Isolates (n)	MDR (n)	MDR (%)	Clinical source
Escherichia coli	22	17	77.3	Urine, blood, wounds
Klebsiella pneumoniae	18	15	83.3	Sputum, urine, blood
Pseudomonas aeruginosa	12	8	66.7	Wounds, burns, ear
Acinetobacter baumannii	8	7	87.5	ICU, endotracheal
Total	60	47	78.3	-

3.6. Antibacterial activity

The composite was clearly more active than its parts (Figure 6, Table 5). Against a representative panel of three reference strains and four clinical MDR/XDR isolates, its MIC ranged from 16 to 64 µg/mL, with a mean of 29.7 µg/mL. For comparison, plain selenium nanoparticles averaged 118.9 µg/mL and chitosan 402.3 µg/mL, so pairing the two cut the MIC about fourfold against selenium alone and more than tenfold against chitosan. The most resistant strain, the XDR *A. baumannii* isolate, still needed only 64 µg/mL. The MBC/MIC ratio was 2 for every isolate, which places the effect firmly in the bactericidal range rather than merely bacteriostatic. These MIC values sit at or below those reported for other green-synthesised selenium and metal nanoparticles against MDR strains [9,22,23,24], and the positive surface charge of the composite is a likely reason for the gain [25]. The species-level pattern is also informative. *P. aeruginosa* and *A. baumannii*, which usually resist more, needed somewhat higher doses than *E. coli* and *K. pneumoniae*, in line with their thicker efflux defences and less permeable envelopes. Even so, the fold difference stayed small, which suggests the composite does not depend on a single entry route that a resistant strain could easily close off. The gain over the separate components is best read as a real cooperative effect: chitosan brings the particle to the negatively charged

surface and loosens the outer membrane, and selenium then does the damage, most likely through reactive oxygen species and thiol binding.

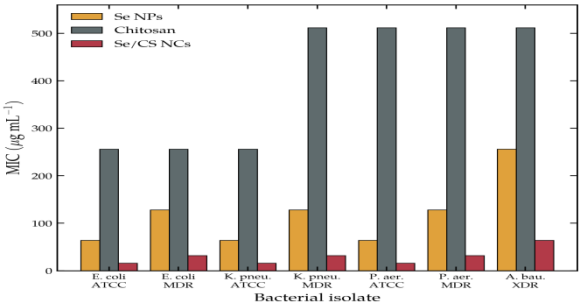

Figure 06: MIC of selenium nanoparticles, chitosan and the Se/CS nanocomposite against the test isolates.

Table 05: MIC and MBC (μg/mL) of selenium nanoparticles, chitosan and the Se/CS nanocomposite.

Isolate	MIC Se NPs	MIC chitosan	MIC Se/CS	MBC Se/CS	MBC/MIC
E. coli ATCC 25922	64	256	16	32	2
E. coli (MDR)	128	256	32	64	2
K. pneumoniae ATCC 700603	64	256	16	32	2
K. pneumoniae (MDR)	128	512	32	64	2
P. aeruginosa ATCC 27853	64	512	16	32	2
P. aeruginosa (MDR)	128	512	32	64	2
A. baumannii (XDR)	256	512	64	128	2
Mean	118.9	402.3	29.7	59.4	2

3.7. Suppression of conjugal transfer

The central question of the study was whether the composite could slow horizontal transfer, and the answer was yes (Figure 7, Table 6). In the untreated control the conjugation frequency was 4.7×10^{-3} transconjugants per recipient. Selenium nanoparticles and chitosan at 1/4 MIC lowered it by 96.0% and 82.6%, useful but partial. The composite was far stronger. At 1/4 MIC the frequency fell to 3.1×10^{-6} (a 99.93% drop), and at 1/2 MIC and the full MIC it reached 1×10^{-8} and 1×10^{-9}. That is a reduction of more than six orders of magnitude at the higher doses. At 1/4 and 1/2 MIC the cultures still grew, so the effect cannot be explained by killing alone, and the composite appears to interfere directly with the transfer process [26]. The full-MIC group is given for completeness only: growth is inhibited at that concentration, so suppression of transfer and suppression of the donor population cannot be separated there. The response was also dose-dependent, with each step up in concentration adding roughly two more logs of suppression. That kind of clean trend argues against a random toxic effect and points to a specific action on the conjugation machinery. It is a useful property in its own right. An agent that lowers transfer at doses below the MIC could, in principle, be used to calm the spread of resistance in a ward or a wound without applying the full selective pressure that drives new resistance.

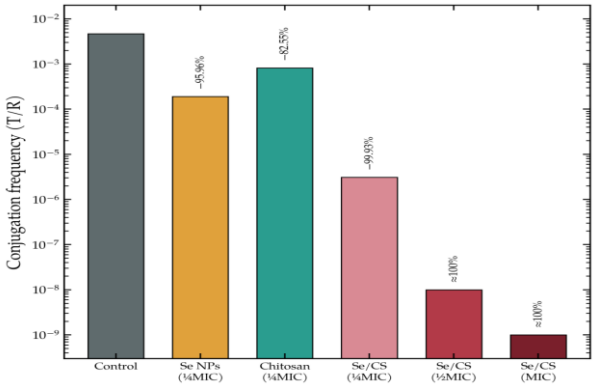

Figure 07: Conjugation frequency under sub-inhibitory treatment on a logarithmic scale.

Table 06: Conjugation frequency (transconjugants per recipient) and its reduction under treatment.

Group	Conjugation frequency (T/R)	Reduction (%)
Control (untreated)	4.7×10^{-3}	0
Se NPs (1/4 MIC)	1.9×10^{-4}	95.96
Chitosan (1/4 MIC)	8.2×10^{-4}	82.55
Se/CS NCs (1/4 MIC)	3.1×10^{-6}	99.93
Se/CS NCs (1/2 MIC)	1.0×10^{-8}	~100
Se/CS NCs (MIC)	1.0×10^{-9}	~100

3.8. Expression of transfer and quorum-sensing genes

RT-qPCR at a sub-inhibitory dose (1/2 MIC) explained the drop in transfer (Figure 8). The core transfer genes

were strongly down-regulated: *traJ* fell to 0.12 of the control, *traA* to 0.13, *traD* to [0.18 / 0.19 - confirm] and *traI* to 0.22 ($p \leq 0.003$; Table 7). *traJ* is a positive regulator of the transfer operon and *traI* is the relaxase that nicks the plasmid before transfer, so silencing them should shut the process at two key steps. In parallel, the negative regulator *finP* rose to 3.21-fold, which would push the operon further towards the off state. The outer-membrane gene *ompA* dropped to 0.48, in line with a less stable envelope and weaker mating-pair formation. The quorum-sensing genes *lasI* and *rhlR* also fell, to 0.39 and 0.42, which matters because quorum sensing helps coordinate conjugation and biofilm behaviour in Gram-negatives [27,28]. Taken together, the composite seems to act on the regulation of transfer, not on a single gene. The link between *traJ* and *finP* is the clearest part of the story. *finP* produces an antisense RNA that keeps *traJ* in check, so a rise in *finP* alongside a fall in *traJ* is a coherent, self-reinforcing switch rather than two unrelated changes. With *traJ* down and *finP* up, the cell simply does not turn the operon on. The lower *traI* adds a second block, because without enough relaxase the plasmid cannot be nicked and prepared for transfer even if a pulus did form. Effects of this size at a sub-lethal dose are hard to get with conventional antibiotics, which tend to select for transfer rather than suppress it.

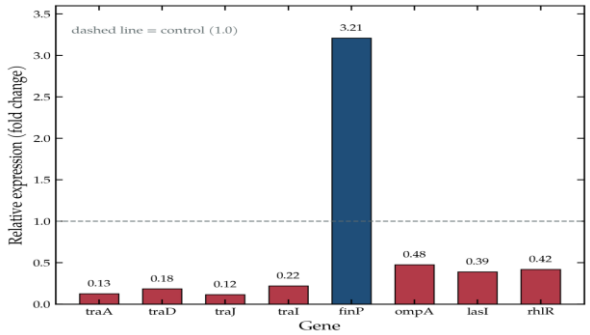

Figure 08: Relative expression of transfer, membrane and quorum-sensing genes at 1/2 MIC (RT-qPCR).

Table 07: Relative expression of the transfer, membrane and quorum-sensing genes at 1/2 MIC (RT-qPCR, $2^{-\Delta\Delta Ct}$ against [reference gene]).

Gene	Function	Fold change vs. control	SD	p
traA	F-pilus subunit	0.13	[SD]	≤ 0.003
traD	Coupling protein	[0.18 / 0.19]	[SD]	≤ 0.003
traI	Relaxase	0.22	[SD]	≤ 0.003
traJ	Positive regulator of the *tra* operon	0.12	[SD]	≤ 0.003
finP	Antisense negative regulator of *traJ*	3.21	[SD]	[p]
ompA	Outer-membrane protein A	0.48	[SD]	[p]
lasI	Quorum sensing (*P. aeruginosa* isolate)	0.39	[SD]	[p]
rhlR	Quorum sensing (*P. aeruginosa* isolate)	0.42	[SD]	[p]

3.9. Resistance genes in transconjugants

The gene-expression data were mirrored at the level of the transferred DNA (Figure 9, Table 8). Before treatment, resistance genes were recovered from transconjugants at high rates: 92% for $bla_{CTX\text{-}M\text{-}15}$, 86% for $bla_{TEM\text{-}1}$ and 82% for *sul1*. After exposure to 1/2 MIC of the composite these rates collapsed, to 4%, 6% and 8%. The carbapenemase genes behaved the same way; $bla_{NDM\text{-}1}$ fell from 42% to 2% and $bla_{OXA\text{-}48}$ from 38% to 1%. Across the nine genes the inhibition of transfer ranged from about 90% to 97%. Blocking the movement of carbapenemase and ESBL genes is the outcome that matters most in practice, since these are the very traits that make current Gram-negative infections so hard to treat [21,29,30,31]. It is also worth noting that the block was broad. Genes for several resistance mechanisms, β-lactam, quinolone, aminoglycoside, sulphonamide and tetracycline, all dropped together. This fits the idea that the composite works on the shared transfer route rather than on any one gene, so it does not matter which resistance cassette a plasmid happens to carry. In a setting where a single plasmid can move a whole package of resistance at once, an agent that closes the route has a clear advantage over one that targets a single product.

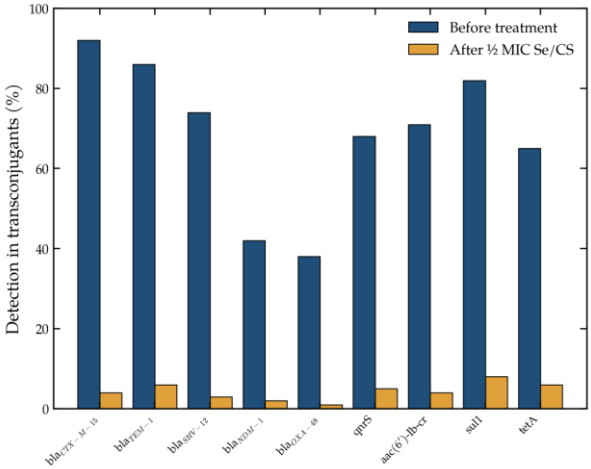

Figure 09: Detection of resistance genes in transconjugants before and after treatment.

Table 08: Detection of resistance genes in transconjugants before and after treatment with 1/2 MIC of the Se/CS nanocomposite.

Gene	Resistance class	Before (%)	After (%)	Reduction (%)
bla$_{CTX-M-15}$	Extended-spectrum β-lactamase	92	4	95.7
bla$_{TEM-1}$	Broad-spectrum β-lactamase	86	6	93.0
bla$_{SHV-12}$	Extended-spectrum β-lactamase	-	-	-
bla$_{NDM-1}$	Metallo-carbapenemase	42	2	95.2
bla$_{OXA-48}$	Carbapenemase	38	1	97.4
qnrS	Quinolone resistance	-	-	-
aac(6')-Ib-cr	Aminoglycoside / quinolone	-	-	-
sul1	Sulphonamide resistance	82	8	90.2
tetA	Tetracycline efflux	-	-	-

3.10. Cytotoxicity and selectivity

A useful antibacterial agent must also spare human cells. In the MTT assay the composite was well tolerated at the concentrations that killed bacteria (Figure 10). Viability of HEK-293 and HFF-1 cells stayed above 90% up to 64 µg/mL and above 82% at 128 µg/mL. Toxicity only became clear at much higher doses, with an IC_{50} of 312 µg/mL. Set against the MIC of 32 µg/mL recorded for most of the MDR clinical isolates in Table 5, this gives a selectivity index of 9.75. An index around or above 10 is generally considered to be a comfortable therapeutic range and it is consistent with the low toxicity described for selenium and chitosan/selenium compounds elsewhere [13]. The two cell lines reacted very similarly, giving credibility to the result. The biological nature of selenium is partially why it is so well tolerated. It is an essential trace element and human cells already possess enzymes to deal with it, but bacteria do not have that buffering and experience the oxidative burden more acutely. The chitosan shell may add a further margin by slowing how fast selenium is released near a host cell. Whatever the exact cause, a window of roughly tenfold between the antibacterial dose and the toxic dose is encouraging for a material meant for topical or surface use.

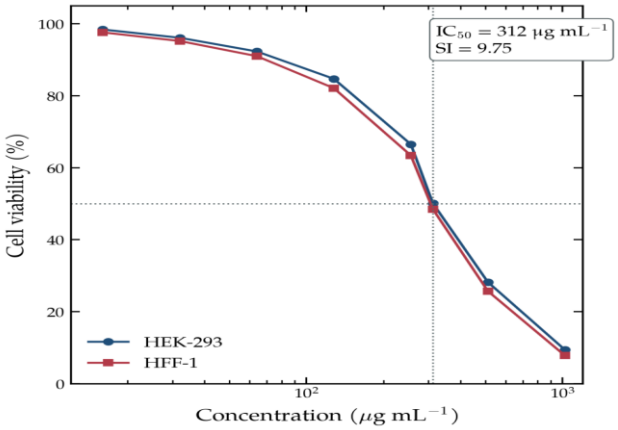

Figure 10: Cytotoxicity of the Se/CS nanocomposite on HEK-293 and HFF-1 cells (MTT).

3.11. Comparison with previous work

Table 9 places the present composite next to recent nanomaterials aimed at resistant bacteria. Most earlier work reports either antibacterial activity or, less often, some effect on gene transfer, but rarely both from one material and against a panel of clinical MDR isolates. The Se/CS NCs described here combine a low MIC, a bactericidal action, a large drop in conjugation and a good selectivity index. The dual action is the main advantage over selenium nanoparticles or chitosan used alone [8,10,12], and over metal nanoparticles that were tested mainly for killing [24].

Table 09: Comparison of representative nanomaterials reported against multidrug-resistant bacteria.

Nanomaterial	Synthesis route	Main target(s)	Key reported effect	Ref.
Se NPs (orange-peel)	Green, biosynthesis	MDR bacteria	Antibacterial + antibiofilm	[8]
Se NPs (Blumea axillaris)	Green, plant extract	MDR aquatic pathogens	Antibacterial	[9]
Se NPs in chitosan	Chemical, colloidal	Oral bacteria	Antibacterial agent	[12]
Chitosan/Se composite	Bioinspired	Bacteria; cells	Antibacterial; low toxicity	[13]
Ag NPs (green)	Green synthesis	Clinical bacteria	Antibacterial + antibiofilm	[23]
Chitosan-coated Au NPs	Chemical	Bacteria	Ciprofloxacin carrier	[24]
Se/CS NCs (this work)	Ascorbic-acid reduction	MDR Gram-negatives	Bactericidal + blocks gene transfer	-

3.12. Proposed mechanism

The results point to a two-part mode of action, sketched in Figure 11. First, the positively charged composite binds the negative outer membrane of Gram-negative cells, disturbs the envelope and, through selenium, promotes oxidative stress; the fall in *ompA* fits this picture. Second, at doses too low to kill, the composite reaches the regulation of conjugation. It represses the *traA*/*traD*/*traI*/*traJ* operon, lifts the brake *finP* and damps quorum sensing, so donor cells can no longer build a working transfer apparatus. The net effect is that resistant cells are killed and, just as important, the plasmids that carry resistance are kept from moving on.

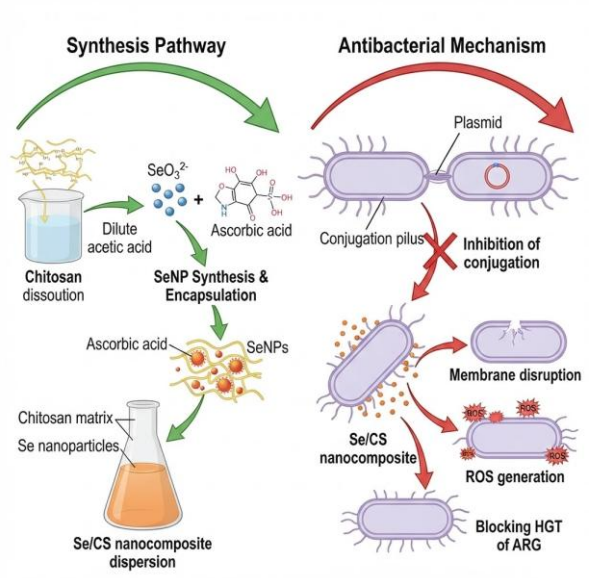

Figure 11: Formation of the Se/CS nanocomposite and its proposed action against resistance dissemination.

3.13. Implications and limitations

The main appeal of this material is that it does two jobs with one agent. It kills resistant Gram-negatives, and at the same time it holds back the transfer that keeps resistance moving through a population. Few reported nanomaterials have been shown to do both against clinical MDR isolates. A positive charge, a modest particle size and a benign chemistry (selenium plus a food-grade polymer) make the composite an attractive starting point for surface coatings, wound dressings or adjuncts to existing drugs.

Some limitations need to be spelt out. The study was in vitro only therefore the levels that inhibit transfer in broth may not be directly relevant to tissue where proteins and pH may alter the function of the particle. The conjugation assay was performed using a specific donor-recipient combination, and other plasmid types may act differently. The gene-expression data suggest that transfer genes decrease, but do not pinpoint the first molecular target targeted by the composite. Open to selection risk for tolerance and conduct in animal models. Stability in the long term. But these are questions for a follow-up study before any therapeutic claim can be made.

4. CONCLUSION

A selenium/chitosan nanocomposite was prepared by a simple ascorbic-acid reduction and characterised by UV-Vis, FTIR, XRD, electron microscopy, DLS, zeta potential and EDX. The data describe semi-spherical, positively charged particles of about 49 nm, built from hexagonal selenium anchored on chitosan. Against a demanding panel of clinical Gram-negative isolates, most of them MDR, the composite was strongly bactericidal, with MIC values well below those of selenium nanoparticles or chitosan alone. Its more striking property was the ability to block horizontal gene transfer. At sub-inhibitory doses it cut plasmid conjugation by more than six orders of magnitude, silenced the *tra* transfer genes, raised *finP* and largely stopped the movement of $bla_{CTX\text{-}M\text{-}15}$, $bla_{NDM\text{-}1}$, $bla_{OXA\text{-}48}$ and other resistance genes into transconjugants. It did all of this while sparing normal human cells, with a selectivity index close to ten. Se/CS NCs therefore deserve further study as a dual-purpose tool that both treats resistant infections and slows the spread of resistance. Work on animal models and on the exact molecular targets is the logical next step.

5. AUTHOR CONTRIBUTIONS

[Author initials] conceived and designed the study. [Author initials] prepared and characterised the nanocomposite. [Author initials] carried out the microbiological and molecular work. [Author initials] analysed the data and wrote the manuscript. All authors read and approved the final version.

6. CONFLICTS OF INTEREST

The authors declare that they have no conflict of interest.

7. DATA AVAILABILITY

The data that support the findings of this study are available from the corresponding author upon reasonable request.

8. ACKNOWLEDGEMENTS

The authors thank [institution/colleagues] for technical assistance. [Funding source, if any.]

9. REFERENCES

1. Murray CJL, Ikuta KS, Sharara F, Swetschinski L, Robles Aguilar G, Gray A, et al. Global burden of bacterial antimicrobial resistance in 2019: a systematic analysis. Lancet. 2022;399(10325):629-655. doi:10.1016/S0140-6736(21)02724-0
2. Nasr P. Genetics, epidemiology, and clinical manifestations of multidrug-resistant *Acinetobacter baumannii*. J Hosp Infect. 2020;104(1):4-11. doi:10.1016/j.jhin.2019.09.021

3. Erdem F, Abulaila A, Aktas Z, Oncul O. In vitro evaluation of double carbapenem and colistin combinations against OXA-48, NDM carbapenemase-producing colistin-resistant *Klebsiella pneumoniae* strains. Antimicrob Resist Infect Control. 2020;9:70. doi:10.1186/s13756-020-00727-4
4. Pinilla-Redondo R, Cyriaque V, Jacquiod S, Sorensen SJ, Riber L. Monitoring plasmid-mediated horizontal gene transfer in microbiomes: recent advances and future perspectives. Plasmid. 2018;99:56-67. doi:10.1016/j.plasmid.2018.08.002
5. Ott LC, Mellata M. Models for gut-mediated horizontal gene transfer by bacterial plasmid conjugation. Front Microbiol. 2022;13:891548. doi:10.3389/fmicb.2022.891548
6. Saba I, Wani K, Batoo KM, Rehman S, Hameed S. Carbon nanomaterials as antimicrobial agents to combat multidrug resistance. In: Nanotechnology Based Strategies for Combating Antimicrobial Resistance. Singapore: Springer; 2024. p. 231-250. doi:10.1007/978-981-97-2023-1_9
7. Rezaee E, Nazari M, Mosayebnia M, Movahed MA. Novel medicinal and synthetic chemistry strategies against antimicrobial resistance. In: Emerging Nanomaterials and Nano-Based Drug Delivery Approaches to Combat Antimicrobial Resistance. Elsevier; 2022. p. 1-34. doi:10.1016/B978-0-323-90792-7.00017-8
8. Salem SS, Badawy MSEM, Al-Askar AA, Arishi AA, Elkady FM, Hashem AH. Green biosynthesis of selenium nanoparticles using orange peel waste: characterization, antibacterial and antibiofilm activities against multidrug-resistant bacteria. Life. 2022;12(6):893. doi:10.3390/life12060893
9. Dash JP, Mani L, Nayak SK. Antibacterial activity of Blumea axillaris synthesized selenium nanoparticles against multidrug resistant pathogens of aquatic origin. Egypt J Basic Appl Sci. 2022;9(1):65-76. doi:10.1080/2314808X.2021.2019949
10. Yilmaz Atay H. Antibacterial activity of chitosan-based systems. In: Functional Chitosan. Singapore: Springer; 2019. p. 457-489. doi:10.1007/978-981-15-0263-7_15
11. Nayak AK, Ahmad SA, Hasnain MS. Chitosan-based nanoparticles in drug delivery. In: Chitosan in Drug Delivery. Elsevier; 2022. p. 55-82. doi:10.1016/B978-0-12-819336-5.00014-5
12. Rangrazi A, Bagheri H, Ghazvini K, Boruziniat A, Darroudi M. Synthesis and antibacterial activity of colloidal selenium nanoparticles in chitosan solution: a new antibacterial agent. Mater Res Express. 2020;6(12):1250h3. doi:10.1088/2053-1591/ab6a56
13. Krishnaraj C, Radhakrishnan S, Ramachandran R, Ramesh T, Kim BS, Yun SI. In vitro toxicological assessment and biosensing potential of bioinspired chitosan nanoparticles, selenium nanoparticles, chitosan/selenium nanocomposites, silver nanoparticles and chitosan/silver nanocomposites. Chemosphere. 2022;301:134790. doi:10.1016/j.chemosphere.2022.134790
14. Sentkowska A, Konarska J, Szmytke J, Grudniak A. Herbal polyphenols as selenium reducers in the green synthesis of selenium nanoparticles: antibacterial and antioxidant capabilities of the obtained SeNPs. Molecules. 2024;29(8):1686. doi:10.3390/molecules29081686
15. Borowska M, Jankowski K. Green synthesis of selenium nanoparticles: characterization and application. In: Handbook of Greener Synthesis of Nanomaterials and Compounds. Elsevier; 2021. p. 171-190. doi:10.1016/B978-0-12-822446-5.00007-1
16. Purohit G, Rawat DS. Characterization techniques for chitosan and its based nanocomposites. In: Chitosan-Based Nanocomposite Materials. Singapore: Springer; 2022. p. 79-101. doi:10.1007/978-981-19-5338-5_3
17. Magiorakos AP, Srinivasan A, Carey RB, Carmeli Y, Falagas ME, Giske CG, et al. Multidrug-resistant, extensively drug-resistant and pandrug-resistant bacteria: an international expert proposal for interim standard definitions for acquired resistance. Clin Microbiol Infect. 2012;18(3):268-281. doi:10.1111/j.1469-0691.2011.03570.x
18. Rodriguez-Grande J, Fernandez-Lopez R. Measuring plasmid conjugation using antibiotic selection. Methods Mol Biol. 2020;2075:93-98. doi:10.1007/978-1-4939-9877-7_6
19. Wang Q, Olesen AK, Maccario L, Madsen JS. An easily modifiable conjugative plasmid for studying horizontal gene transfer. Plasmid. 2022;123-124:102649. doi:10.1016/j.plasmid.2022.102649
20. Tarassoli Z, Najjar R, Amani A. Formulation and optimization of lemon balm extract loaded azelaic acid-chitosan nanoparticles for antibacterial applications. J Drug Deliv Sci Technol. 2021;65:102687. doi:10.1016/j.jddst.2021.102687
21. Ghanbarinasab F, Haeili M, Nasiri Ghanati S, Moghimi M. High prevalence of OXA-48-like and NDM carbapenemases among carbapenem resistant *Klebsiella pneumoniae* of clinical origin from Iran. Iran J Microbiol. 2023;15(5):609-615. doi:10.18502/ijm.v15i5.13866
22. Nataraj M, Carmelin DS, Sravanthy PG, Saravanan M. Evaluation of antibacterial efficacy of Centella asiatica-mediated selenium oxide nanoparticles against multidrug-resistant upper respiratory isolates. Cureus. 2024;16(4):e58350. doi:10.7759/cureus.58350
23. Hammadi NN, Hasson SO, Al-Awady MJ. Synergistic antibacterial activity of green-synthesized selenium nanoparticles and probiotics against multidrug-resistant pathogens. Microbes Infect Dis. 2026. doi:10.21608/mid.2026.460488.3654

24. Barabadi H, Mojab F, Vahidi H, Marashi B, Talank N, Hosseini O, et al. Green synthesis, characterization, antibacterial and biofilm inhibitory activity of silver nanoparticles compared to commercial silver nanoparticles. Inorg Chem Commun. 2021;129:108647. doi:10.1016/j.inoche.2021.108647
25. Amrish Varshan GS, Namasivayam SKR, Sowmya R, Sivasuriyan KS. Ciprofloxacin-loaded chitosan-coated gold nanoparticles: antibacterial activity and molecular interaction analysis. J Drug Deliv Sci Technol. 2026;126:108736. doi:10.1016/j.jddst.2026.108736
26. Ott LC, Mellata M. Short-chain fatty acids inhibit bacterial plasmid transfer through conjugation *in vitro* and in *ex vivo* chicken tissue explants. Front Microbiol. 2024;15:1414401. doi:10.3389/fmicb.2024.1414401
27. Kenoosh HA, Shehan MA. Quenching of virulence factors and expression of *lasI* and *rhlR* genes of quorum sensing by natural compounds in *Pseudomonas aeruginosa* isolates. Int J Health Sci. 2022;6(S6):2827-2834. doi:10.53730/ijhs.v6nS6.9813
28. Gokalsin B, Berber D, Sesal NC. *Pseudomonas aeruginosa* quorum sensing and biofilm inhibition. In: Quorum Sensing. Elsevier; 2019. p. 227-256. doi:10.1016/B978-0-12-814905-8.00009-5
29. Allander L, Vickberg K, Lagerback P, Sandegren L, Tangden T. Evaluation of *in vitro* activity of double-carbapenem combinations against KPC-2-, OXA-48- and NDM-producing *Escherichia coli* and *Klebsiella pneumoniae*. Antibiotics. 2022;11(11):1646. doi:10.3390/antibiotics11111646
30. Bozorgi Mohajer H, Salimizand H, Gharanizadeh D, Hossainpanahi A, Ramazanzadeh R. Investigation of NDM-1 and OXA-48 producing carbapenem resistant *Klebsiella pneumoniae* ST15 in Iran. Acta Microbiol Immunol Hung. 2023;70(1):38-46. doi:10.1556/030.2023.01945
31. Sanikhani R, Akbari M, Hosseinzadeh M, Siavash M, Badmasti F, Solgi H. Outbreak of colistin and carbapenem-resistant *Klebsiella pneumoniae* ST16 co-producing NDM-1 and OXA-48 isolates in an Iranian hospital. BMC Microbiol. 2024;24:53. doi:10.1186/s12866-024-03207-6